



## Supported ionic liquid-like phases based on CMS/DVB with different NR<sub>3</sub> cations as catalysts for the chlorosilanes disproportionation

Andrey V. Vorotyntsev<sup>a,\*</sup>, Anton N. Petukhov<sup>a</sup>, Dmitriy A. Makarov<sup>a</sup>, Tatyana S. Sazanova<sup>a</sup>, Evgeny N. Razov<sup>b</sup>, Alexander V. Nyuchev<sup>c</sup>, Leonid A. Mochalov<sup>a</sup>, Artem N. Markov<sup>a</sup>, Artem D. Kulikov<sup>a</sup>, Vladimir M. Vorotyntsev<sup>a</sup>

<sup>a</sup> Nizhny Novgorod State Technical University n.a. R.E. Alekseev, Nanotechnology and Biotechnology Department, Laboratory of Membrane and Catalytic Processes, Nizhny Novgorod, 603950, Russian Federation

<sup>b</sup> Institute for Problems in Mechanical Engineering, Russian Academy of Sciences, Nizhny Novgorod, 603024, Russian Federation

<sup>c</sup> N.I. Lobachevsky State University of Nizhny Novgorod, Nizhny Novgorod, 603950, Russian Federation



### ARTICLE INFO

#### Keywords:

Trichlorosilane  
Disproportionation  
Supported ionic liquid-like phases  
Silane  
Heterogeneous catalysis

### ABSTRACT

The variety of catalysts based on macroporous supported ionic liquid-like phases using chloromethyl styrene cross-linked with divinylbenzene (CMS/DVB) and different NR<sub>3</sub> cations was investigated for disproportionation of trichlorosilane in a continuous-flow reactor. To determine the optimal conditions for conducting a complex catalytic process, the primary task is to determine the thermodynamical equilibrium state of the reaction system. Increase in the concentration of DCS in the system occurs from 5 to 10%, which in turn is promising in terms of considering DCS as the main precursor for the processes of epitaxial silicon growth. In addition, the maximum attainable temperature is thermodynamically optimal for the process. In the first stage, the thermal stability of the catalyst supports was determined using evolved gas analysis and all samples have a similar thermal stability 475 K. All samples have been carefully studied by SEM, AFM, EGA and nitrogen physisorption. To compare the catalytic activity of different catalytic systems on the basis of macroporous supports modified by different tricatic ammonium functional groups with the subsequent activation, the kinetics of the TCS disproportionation on the catalyst sample having the highest catalytic activity was studied. The results obtained indicate that the introduction of acceptor substituents increases catalytic activity in the disproportionation of TCS. To assess the feasibility of using dichlorosilane (DCS) as a raw material for the creation of semiconductor structures, the kinetics of thermal decomposition of DCS in a mixture with hydrogen was studied at a temperature of 1200–1500 K. According to the obtained kinetic results, the activation energy of the process is determined, which is in the temperature range of 1220–1320 K and the concentration of DCS in hydrogen 9–28.6 mol.%, is 112.9 kJ/mol. Activation energy value indicates the kinetical mode of the thermal decomposition.

### 1. Introduction

Currently, due to the development of solar energy (the annual increase in demand for the production of solar panels is about 35–45% in 2010–2018 [1]), as well as the micro- and nanoelectronics industry the consumption of high-purity polycrystalline silicon increases every year, therefore, there is an obvious need to reduce its cost, as well as to increase the industrial and environmental safety of its production. In addition, the development of industry leads to an increase in demand for electricity and an increase in the capacity of extraction and processing of organic energy sources, which threatens environmental

safety. Thus, it is extremely important to look for alternative environmentally friendly renewable energy sources, one of which is photovoltaics. The basic type of raw materials for the production of solar energy components is polycrystalline silicon [2–9] (Fig. 1).

The main technological process for producing polysilicon is hydrochlorination of technical silicon (Siemens process) to trichlorosilane (TCS), its separation from the vapor-gas mixture, followed by hydrogen reduction of TCS to polysilicon. However, in the implementation process a rather significant amount of side product (total of 1 ton of polysilicon as a by-product produces up to 18 tons of a highly toxic product - silicon tetrachloride (hazard class 3 NFPA 704) is formed, the

\* Corresponding author at: Nizhny Novgorod State Technical University n.a. R.E. Alekseev, Nanotechnology and Biotechnology Department, Laboratory of Membrane and Catalytic Processes, Minina str. 24, Nizhny Novgorod, 603950, Russian Federation.

E-mail address: [an.vorotyntsev@gmail.com](mailto:an.vorotyntsev@gmail.com) (A.V. Vorotyntsev).

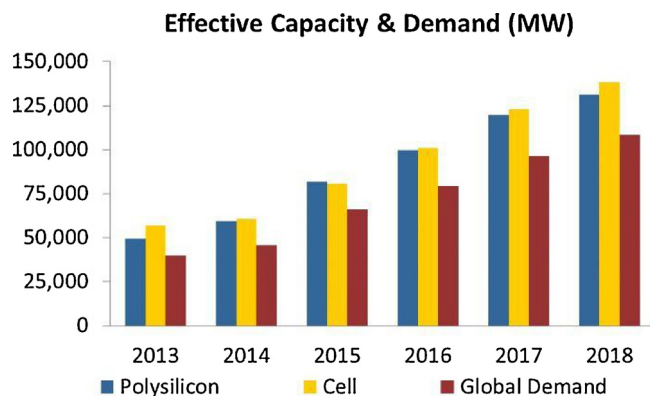


Fig. 1. The current forecast for module supply annually, out to the end of 2018, where historic data back to 2013 is displayed for legacy demand comparisons.

process has a high level of energy consumption (process temperature - 1473 K) and, as a consequence, high production costs and difficulties in obtaining polysilicon of electronic-grade purity [10–14].

In addition, in recent years, a method of manufacturing polycrystalline silicon by thermal decomposition of monosilane (Union carbide process) has been widely used in the industry, which attracts increasing attention, since it has an attractive level of investment costs, low energy consumption (due to low reaction temperatures – 353 K) and significantly less environmental pollution to producing solar-grade polysilicon. Monosilane (MS) is widely used in the opto-, micro- and nanoelectronics industries to produce a variety of semiconductor structures. MS is largely obtained by catalytic disproportionation of TCS. However, the main problem of this method is a sufficiently large yield of a by-product - silicon tetrachloride [15] (up to 16 tons of tetrachloride per 1 ton of polysilicon), and MS pollution by electroactive impurities from catalysts [16–21].

Thus, today the issue of improving the technology of catalytic disproportionation of TCS, in terms of increasing the yield and selectivity of MS with the use of reaction-rectification technology [22–25], as well as reducing the yield of silicon tetrachloride (STC) through the implementation of the recycling is quite acute.

Reducing process temperature, increasing the degree of conversion and selectivity, as well as reducing the level of impurity composition, which can be solved by finding new, more stable catalytic systems, is the basic innovative way to improve the traditional production of polycrystalline silicon in order to reduce its cost in the market.

In addition, in recent years the attention of researchers was attracted to the dichlorosilane (DCS) [26]. The advantages of its use are lowering the temperature and increasing the rate of thermal decomposition in the processes of epitaxial silicon growth. DCS was the main application in microelectronics [27–29], but its use for obtaining bulk silicon crystals is also promising.

Among the known methods for the synthesis of DCS of greatest interest is the reaction of disproportionation of TCS, but the process of disproportionation is not completed at the stage of DCS formation and STC, it's characterized by a system of three series-parallel reactions:



Currently, in the reaction of dispersion of TCS, catalytic active anion exchange resins containing tertiary amine or Quaternary ammonium groups are usually used [30–35]. If we look at the equations of reactions (1)–(3), then we can see that monosilane is obtained in the last stage, and dichlorosilane in (1) and (3) stages. Thus, at the final, we have a low yield of monosilane. From this point of view, the substitution of monosilane to dichlorosilane, as a raw material for the production of

polycrystalline silicon, is potentially interesting from the economic point (the monosilane yield reaches 10%, compared with monosilane, whose yield reaches 0.4%) and the ecological point (the production of dichlorosilane reduces the yield of silicon tetrachloride by almost 3 times).

However, recently [36–38] creation of heterogeneous catalytic systems on the basis of ionic liquids (IL) covalently bound with the porous support (SILLPs - supported ionic liquid-like phases), causes rather strong interest. A distinctive feature of the catalytic systems obtained is their proximity in properties to molecular catalysts, with homogeneous active sites, which largely provides a high selectivity. In SILLPs technology, the key factor is not only the properties and activity of the functional group but also the texture characteristics of the porous support, such as specific surface area, average particle diameter, pore size distribution and surface morphology [39–42,45].

The main purpose of this work is the preparation of supported ionic liquid-like phases (SILLPs) by the modification of macroporous and gel type divinylbenzene – chloromethyl styrene (DVB-CMS) microspheres [43]. Our approach was based on the immobilization by covalent binding of IL - like units when ILs properties are transferred to the solid phase with similar characteristics than the homogeneous analogs [44,45]. Since these catalytic systems with control solid nature enable them to be used in the development of  $\mu$ -reactors for continuous processes, the determination of their catalytically active in the disproportionation of TCS to obtain the main product of DCS was carefully studied.

## 2. Experimental

### 2.1. Materials

Divinylbenzene (DVB), chloromethyl styrene (CMS), Chloroethane solution 2.0 M in tert-butyl methyl ether, anhydrous, Dimethylamine solution 40 wt. % in  $\text{H}_2\text{O}$ , Trimethylamine solution ~ 45 wt. % in  $\text{H}_2\text{O}$  (T) (Sigma-Aldrich Corp., Germany). Hydrochloric acid, sodium chloride, poly(vinyl alcohol) (PVA), and solvents (Vekton Ltd., Russia). 2,2'-Azobisisobutyronitrile (AIBN) (Chemical Line Ltd., Russia). All reagents and solvents were used without further purification. For the disproportionation of TCS, we used the initial substances: Trichlorosilane 99.998%, (Firm HORST Ltd., Russia), Helium 99,99999% and Hydrogen chloride 99.99998%, (Monitoring Ltd., Russia).

### 2.2. Support catalyst synthesis

DVB/CMS copolymer beads were obtained by suspension copolymerization of 4 ml DVB and 8 ml CMS along with 10, 100 and 200% (with respect to the organic phase) mixture of heptane and toluene as a porogen in 3% NaCl, 3% PVA (w/w) water solution (0.130 g of AIBN was used to initiate the reaction). The reaction was carried out at 75 °C in the ultrasonic bath under stirring. After 8 h, the product was thrice washed with hot water and twice with ethanol to remove PVA from its surface, then other impurities, porogen, and unreacted monomers were extracted using Soxhlet apparatus (1 day in acetone, 2 days in ethanol). After extraction polymer beads were dried in the vacuum oven (10 mbar) for 3 days at 50 °C.

### 2.3. SILLPs synthesis through the direct functionalization of DVB/CMS beads

The functionalization of the obtained DVB/CMS supports was carried out in accordance with Fig. 2.

DVB/CMS copolymer beads were stirred with 1.2 equivalents of the corresponding amine (based on the CMS amount) water solution in ethanol to give di- and trimethyl-substituted quaternary ammonium chloride at 80 °C for 48 h then washed with ethanol in the Soxhlet

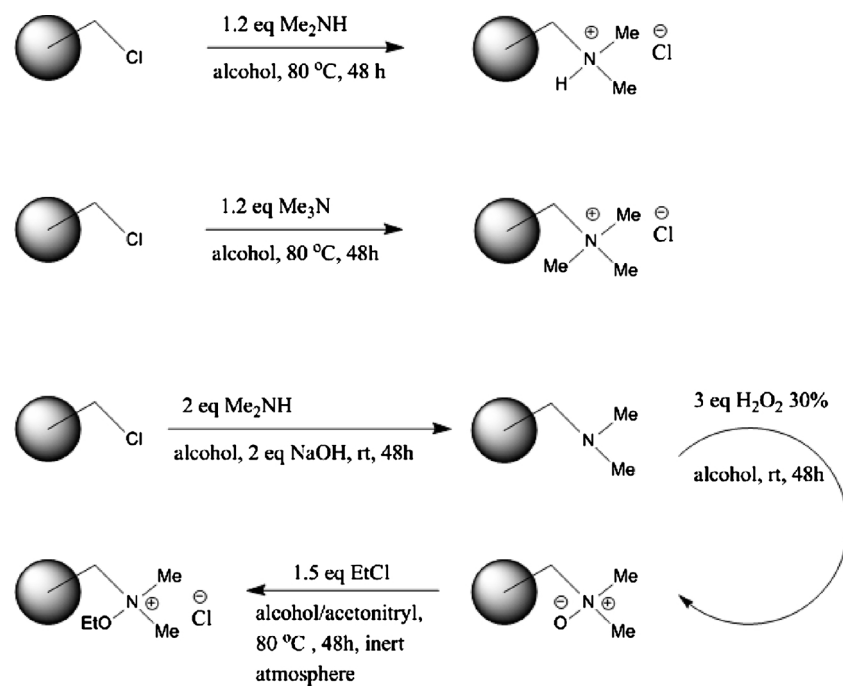


Fig. 2. Schematic representation of direct functionalization of DVB/CMS beads.

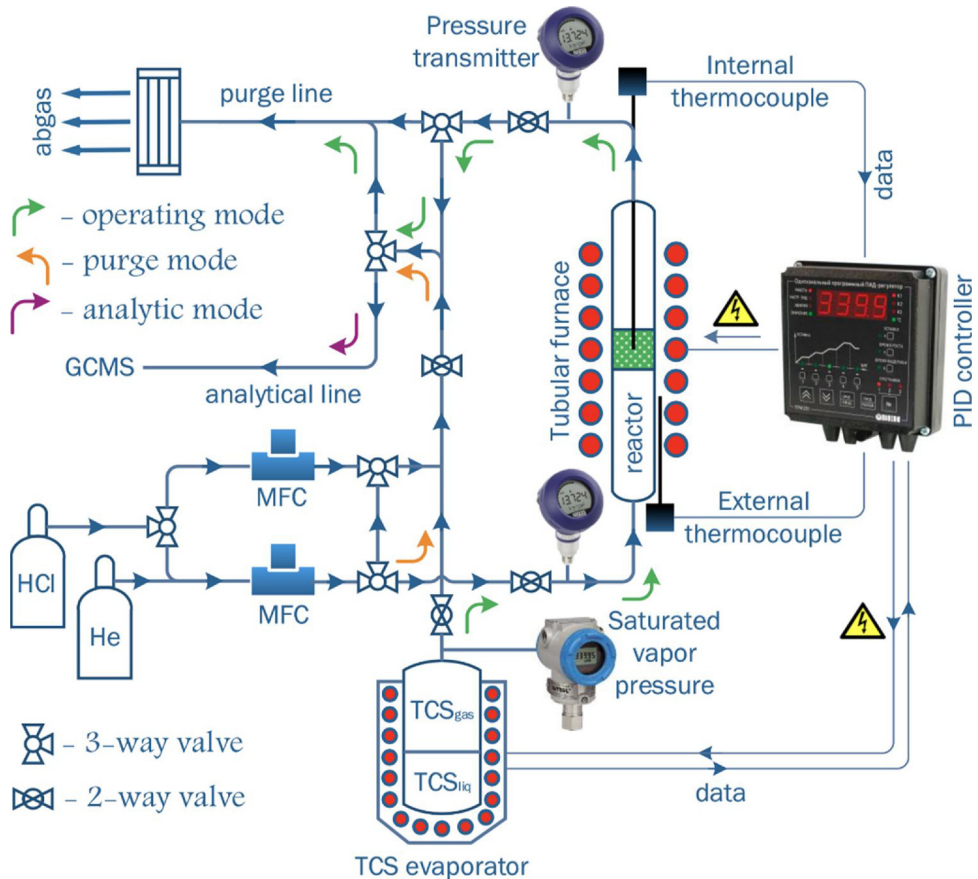


Fig. 3. Apparatus for investigation of the disproportionation of TCS.

apparatus for 8 h and then dried in the vacuum oven at 50 °C for 3 days. In order to synthesize dimethyl ethoxy - substituted quaternary ammonium chloride, initial polymer beads were stirred with 2 equivalents of dimethylamine and 2 equivalents of sodium hydroxide in ethanol at 80 °C for 48 h, then the SILC was washed with ethanol in the Soxhlet

apparatus for 8 h, stirred with 3 equivalents of hydrogen peroxide in ethanol at room temperature for another 48 h, washed with ethanol in the Soxhlet apparatus for 8 h again, stirred with 1.5 equivalents of chloromethane ether solution with ethanol and acetonitrile as solvents in nitrogen atmosphere at 80 °C for 48 h, and finally washed with

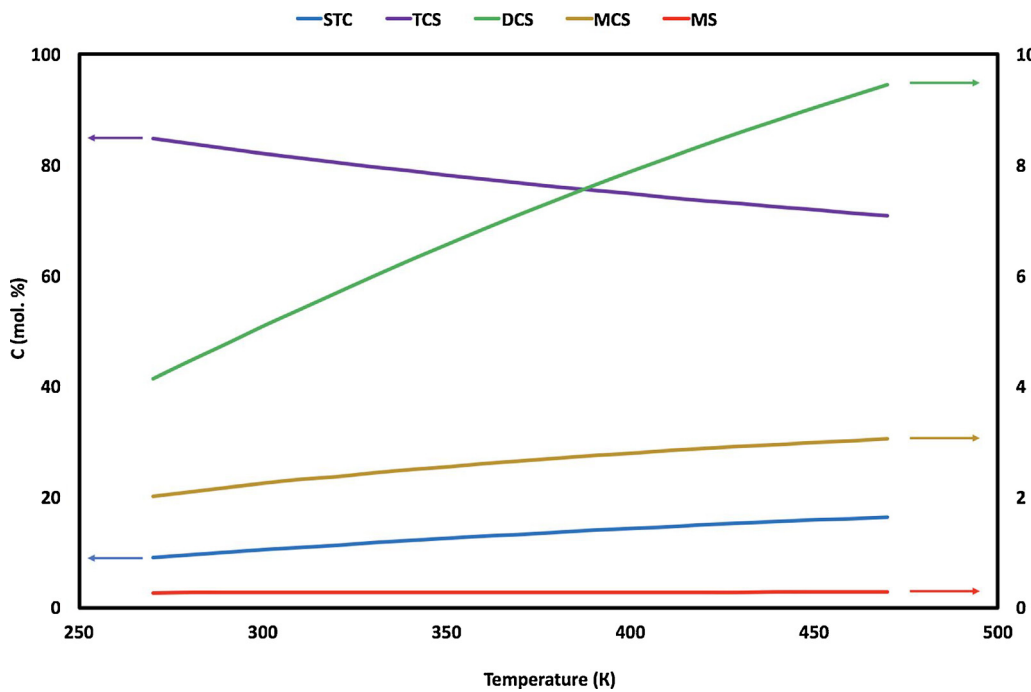


Fig. 4. Temperature dependence of the equilibrium yield of chlorosilanes in disproportion of TCS in the vapor phase.

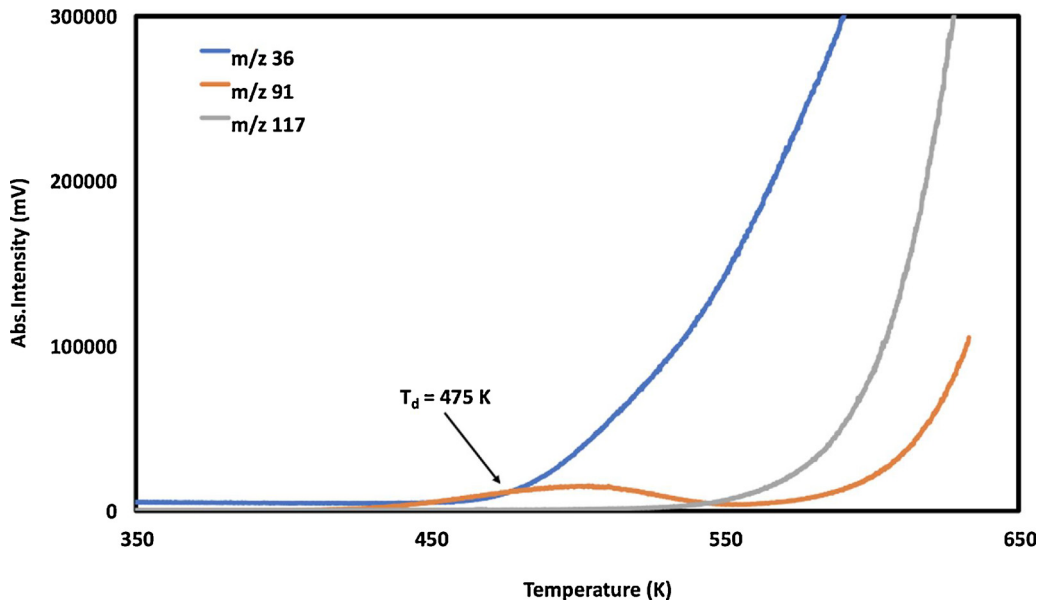


Fig. 5. Thermal stability DVB/CMS beads from temperature 350 to 650 K.

ethanol in Soxhlet apparatus for 8 h and dried in vacuum oven at 50 °C for 3 days.

#### 2.4. Determination of the full static volumetric capacity

The ion exchange capacity of the pellicular resins was determined by titration. Following the IUPAC recommendations [44], the resins were converted to the chloride-form (Cl-form) and the ion exchange capacity was determined by titration with a standard aqueous  $\text{AgNO}_3$  solution.

#### 2.5. Adsorption-desorption isotherms and pore size distribution

Study of the porous structure of mesoporous supports based on DVB/CMS was conducted on the Sorbi – MS (Meta Ltd., Russia) with

advanced term training of samples. The study of solids is closely related to the interpretation of the IV type of adsorption isotherms, where there is a hysteresis loop. By interpreting this type of isotherms, it is possible to estimate the specific surface area by BET and STSA with acceptable accuracy, as well as to obtain an approximate characteristic of pore size distribution and full pore volume. The method is based on Thomson's equation [45], which was later modified by Kelvin:

$$\ln(p/p_0) = -\frac{2\gamma V_L}{r_m RT} \quad (4)$$

where  $P/P_0$  – the relative partial pressure of a vapor in equilibrium with a meniscus having a radius of curvature  $r_m$ ;  $\gamma$  and  $V_L$  – the surface tension and molar volume of the liquid adsorbent, respectively,  $R$  and  $T$  – applied in their usual value.

Using the Kelvin equation, it is possible to calculate the minimum

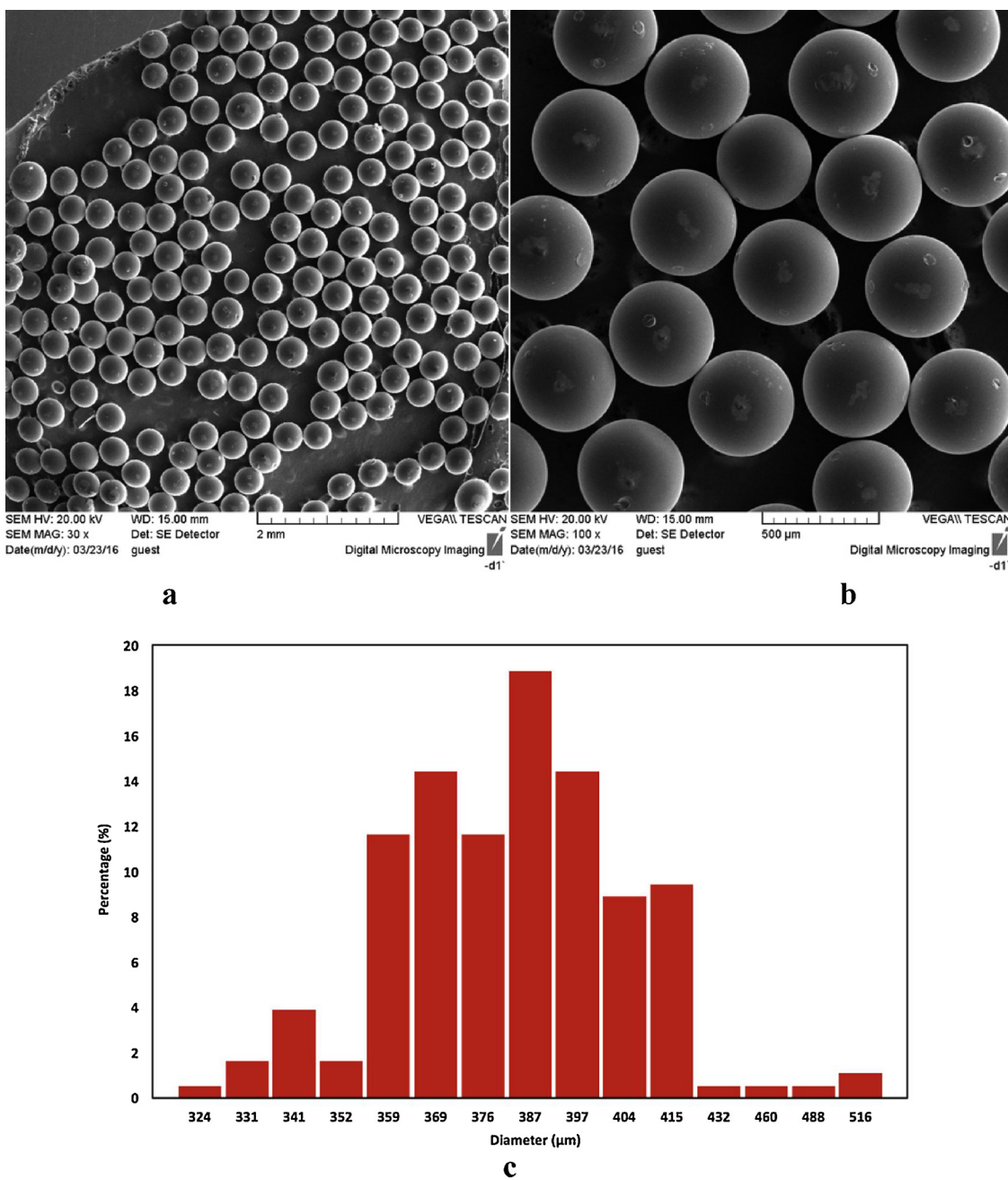


Fig. 6. SEM micrographs of the DVB/CMS beads a – 30 x, b – 100 x, c - particle size distribution.

radius of pores in which capillary condensation takes place at the hysteresis loop base point. The long-term practice has shown that this minimum radius depends on the nature of the sample, but it is rarely less than  $\sim 1$  nm. To simplify the calculations, a model of cylindrical pores was chosen, which is typical for spherical particles.

#### 2.6. Products GCMS analysis

«Ex-situ» qualitative analysis of the major reaction products was carried out on GCMS – QP2010Plus (Shimadzu, Japan) with a vacuum sample inlet system through automatic injection valve (Valco Instruments Co Inc, USA). The products which were obtained in the reaction were separated on the Agilent capillary column CP-7434 Select Silanes<sup>TM</sup> (60 m, film 2,0  $\mu$ m) with a stationary phase based on trifluoropropylmethylpolysiloxane at 323 K for 10 min; carrier gas – helium. Reaction products were identified with the help of NIST-11

database of mass spectra and on the basis of the  $m/z$  of the formed fragments and «GCMS Real Time Analysis» software. According the obtained data the main products were consisted of  $\text{SiH}_4$  ( $m/z$  30),  $\text{SiH}_3\text{Cl}$  ( $m/z$  64),  $\text{SiH}_2\text{Cl}_2$  ( $m/z$  99),  $\text{SiHCl}_3$  ( $m/z$  133),  $\text{SiCl}_4$  ( $m/z$  170) with the help of select ion monitoring (SIM) mode in the mass spectrometer.

#### 2.7. Structure AFM/SEM analysis

The surface structure of the microspheres was studied by a scanning probe microscope SPM-9700 (Shimadzu, Japan). A maximal lateral scan area of AFM piezoelectric scanner was  $30 \mu\text{m} \times 30 \mu\text{m}$ . The scans were data arrays with a dimension of  $256 \times 256$  pixels. The probe sensitivity and the scanner accuracy of the atomic force microscope allowed to obtain surface images with a lateral resolution to 0.2 nm and a vertical resolution to 0.01 nm. Approximation levels were  $30 \mu\text{m}$ ,

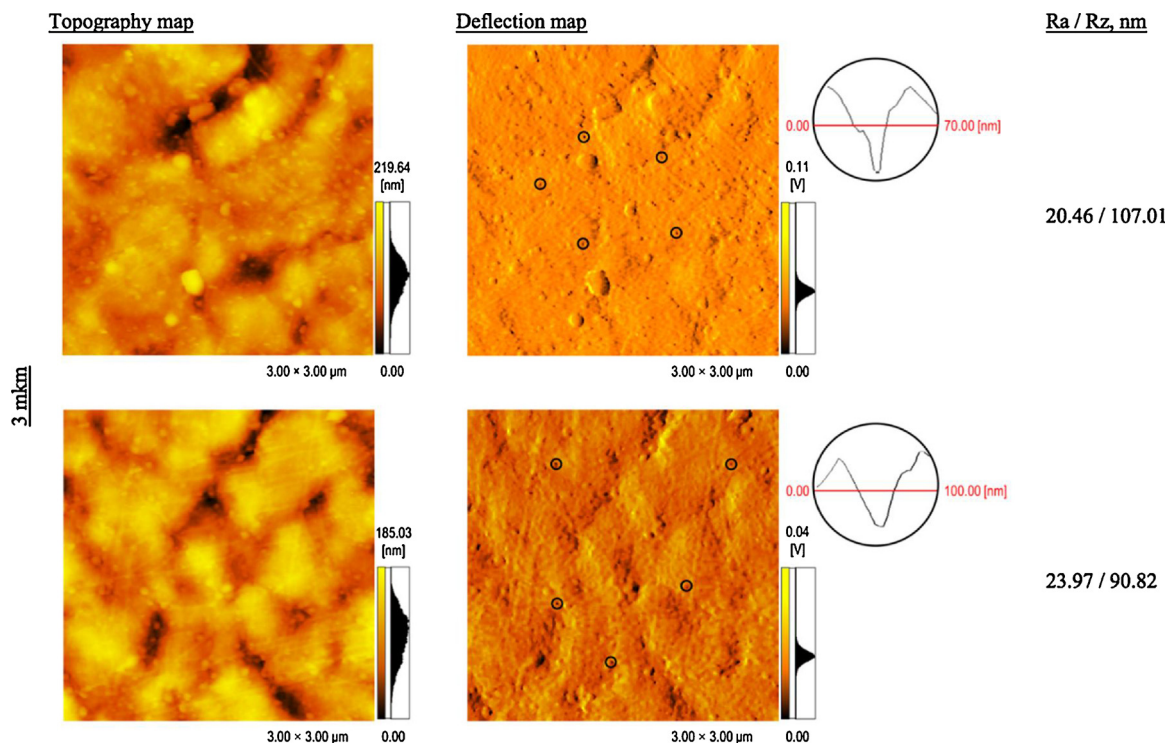


Fig. 7. AFM images of the microsphere surface and deflection map.

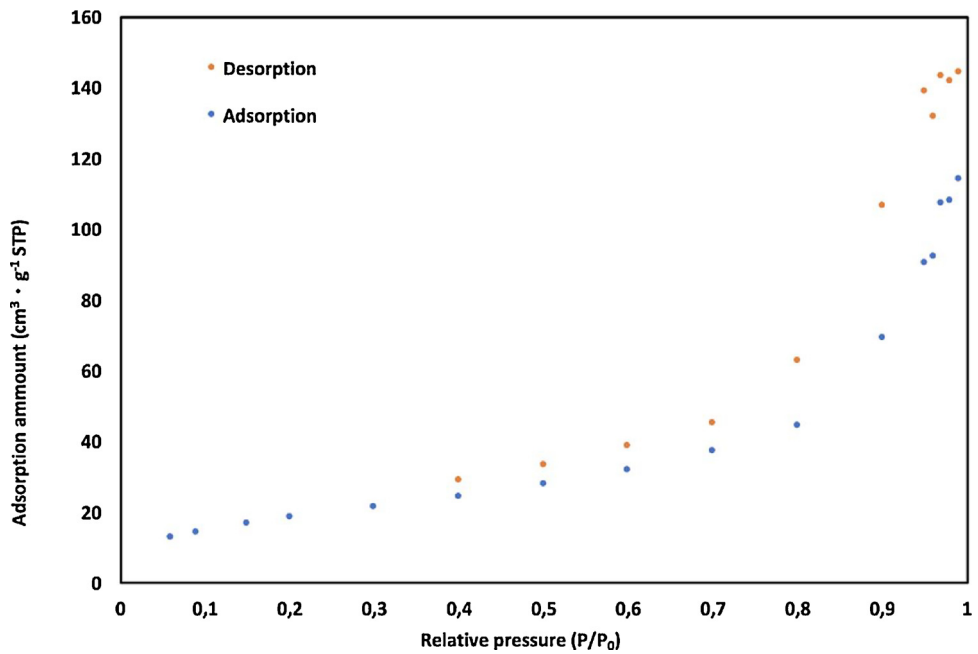


Fig. 8. Nitrogen adsorption-desorption isotherms at 77 K.

10  $\mu\text{m}$  and 3  $\mu\text{m}$ . For checking purposes of reproducibility, the samples were scanned on different sites of their surface. The experiments were carried out under ambient conditions. To eliminate possible crosstalk artifacts (image defects due to crosstalk scanner), software corrective filters were used. In addition, automatic correction of linear noise was applied during scanning.

The microsphere samples preparation was carried out by their fixation to a special holder using adhesive carbon tabs (SPI Supplies Division of Structure Probe Inc., USA) and cleaning of their surface out of dust with ethanol.

Since polymeric surfaces have a loosely-coupled structure, AFM

scanning was performed using a tapping mode by silicon vibrating cantilevers POINTPROBE FMR-20 (Nano World Innovative Technologies, USA) with a stiffness coefficient of 1.3  $\text{N m}^{-1}$  and a typical tip radius of no more than 8 nm (guaranteed – no more than 12 nm), a tip height was from 10 to 15 microns.

A deflection image, which is the first derivative of the topography image, on a softer sample (like polymers, DNA, and biological cells) often reveals sub-surface structure more clearly than a topography image, so digital imaging of the measurement results consisted in the representation of both topographic and deflection maps. Processing of the obtained AFM images and their analysis were performed by a

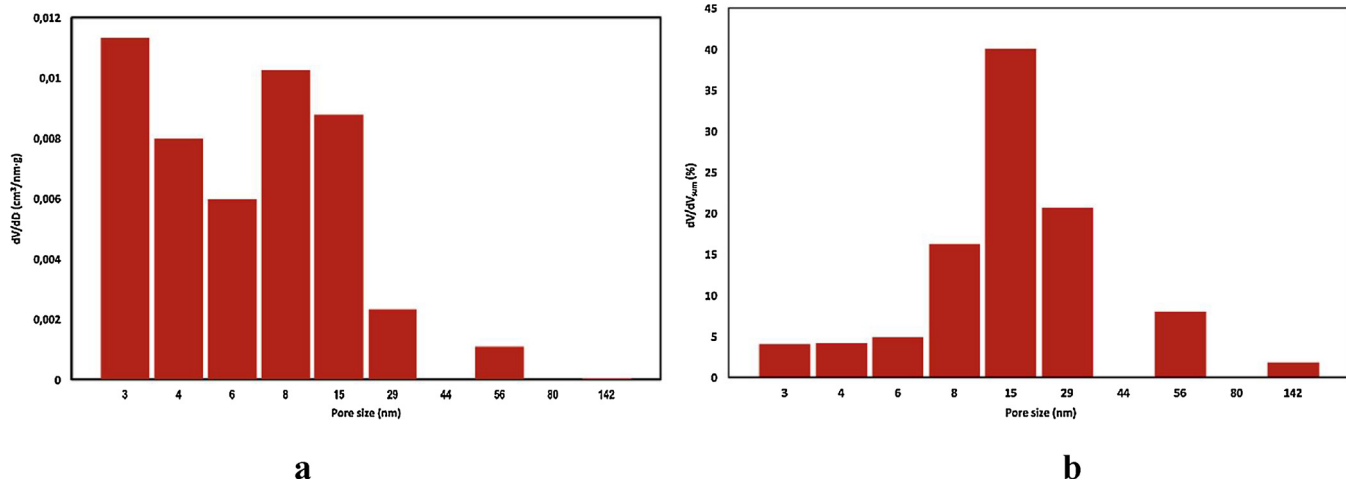


Fig. 9. Pore size distribution (a - full pore size distribution, b - pore size distribution of relative total volume).

Table 1  
Structural characteristics DVB/CMS beads with the various volume of porogen.

Sample	$S^{\text{BET}}$ , $\text{m}^2/\text{g}$	Pore volume, $\text{cc}/\text{g}$	Average pore diameter, nm
DVB/CMS (10 % porogen)	5	0,027	3.5
DVB/CMS (100 % porogen)	52	0.164	14.9
DVB/CMS (200 % porogen)	85	0,223	29.4

Table 2  
Structural properties and catalytic activity of the various samples.

No	Sample	Functional Group <sup>a</sup>	Exchange capacity (meq/g)	$S^{\text{BET}}$ ( $\text{m}^2/\text{g}$ )	K ( $\text{s}^{-1} \text{cm}^{-3}$ )
1	DVB/CMS_N	$\text{S}-\text{N}(\text{CH}_3)_3$	3.2	5	–
2	(Me) <sub>3</sub>		3.5	54	0.009
3			3.4	70	0.041
4	DVB/CMS_N	$\text{S}-\text{N}(\text{CH}_3)_2\text{EtO}$	3.8	3	0.019
5	(Me) <sub>2</sub> EtO		3.6	52	0.84
6			3.9	79	1
7	DVB/CMS_N	$\text{S}-\text{NH}(\text{CH}_3)_2$	3.6	2	0.016
8	(Me) <sub>2</sub> H		3.3	45	0.062
9			3.5	78	0.85

<sup>a</sup> S – support, in all samples as an anion –  $\text{Cl}^-$ .

software SPM Manager ver. 4.02 (Shimadzu, Japan).

The morphological and visual appearance characteristics were observed by scanning electron microscopy Vega II (Tescan, Czech Republic) at the voltage of 20 kV with backscattered electron (BSE) detector and detector of reflected electrons (RE detector) with zooming from 500 to 8000 and 20,000. The use of BSE and RE detectors allows obtaining the most contrast images in comparison with SE detector.

### 2.8. Evolved gas-analysis (EGA)

Thermodesorption analysis for coupled evolved gas-analysis (Direct EGA-MS) measurements was carried out on the temperature-programmable Double-Shot Pyrolyzer EGA/PY-3030D (Frontier Laboratories, Japan) incorporated in GCMS QP-2010Plus (Shimadzu, Japan). To perform an experiment, a deactivated stainless-steel sample cup loaded with approximately 100  $\mu\text{g}$  of the sample was dropped into a quartz pyrolysis tube. The quartz tube was surrounded by a tubular furnace, which provided uniform heating and maintained the pyrolysis temperature in accordance with the following temperature program under

the helium flow at 50 ml/min, at the pyrolyzer was reduced to 1 ml/min at the capillary column by means of a splitter: the first stage – holding at 323 K for 10 min, after that, at the 2nd stage the sample was heating in the range of 323–773 K (10 K/min). During the second stage, identification of the resulting chromatographic peaks was carried out with the help of a mass selective detector. Ionization in the mass-spectrometer was carried out by electron ionization (EI) at 70 eV and a mass range between 12 and 500 amu. scanned at a rate of 2000s/scan. Reaction products were separated on 2,5 m Tube made of Ultra ALLOY EGA (Frontier Laboratories, Japan) at 373 K (45 min) with the help of selected ion monitoring, carrier gas – helium.

### 2.9. Apparatus

For the preparation of the vapor-gas of the mixture which is fed to the reactor an evaporator was used (Fig. 3) in which carrier gas passes through the gas phase TCS and saturated with vapor. The carrier gas flow rate for each ratio rate was 1–15 ml/min. The concentration of components in the vapor-gas of the mixture can be changed by the temperature of the evaporator with TCS and the flow rate of the carrier gas.

A stainless-steel cylinder with a length of 470 mm and an inner diameter of 6 mm with Fitok ferrule union 3/8"–1/4" was used as the continuous flow reactor for carrying out the catalytic disproportionation of TCS. The reactor was designed to allow quick assembly and disassembly so as to examine the catalytic activity of the catalysts. In the experimental research, the reactor temperature varied within the range of 333 K and 423 K. The catalyst was put into the reactor, then purged with a carrier gas with gradual heating from 298 K to 423 K, followed by treatment with a mixture of TCS with a carrier gas at the experimental temperature.

## 3. Results and discussion

### 3.1. Thermodynamic analysis

To determine the optimal conditions for conducting a complex catalytic process, the primary task is to determine the thermodynamical equilibrium state of the reaction system. Equilibrium concentrations of chlorosilanes in the reaction system in the gas phase described by equations (1)–(3) were calculated to determine the thermodynamically probable yield of products of the dispersion reaction (Fig. 4). It was shown that the concentration of DCS in the equilibrium mixture increases with the temperature and is practically independent of the pressure and phase composition of the system. The calculation of the temperature dependence of the equilibrium composition was carried

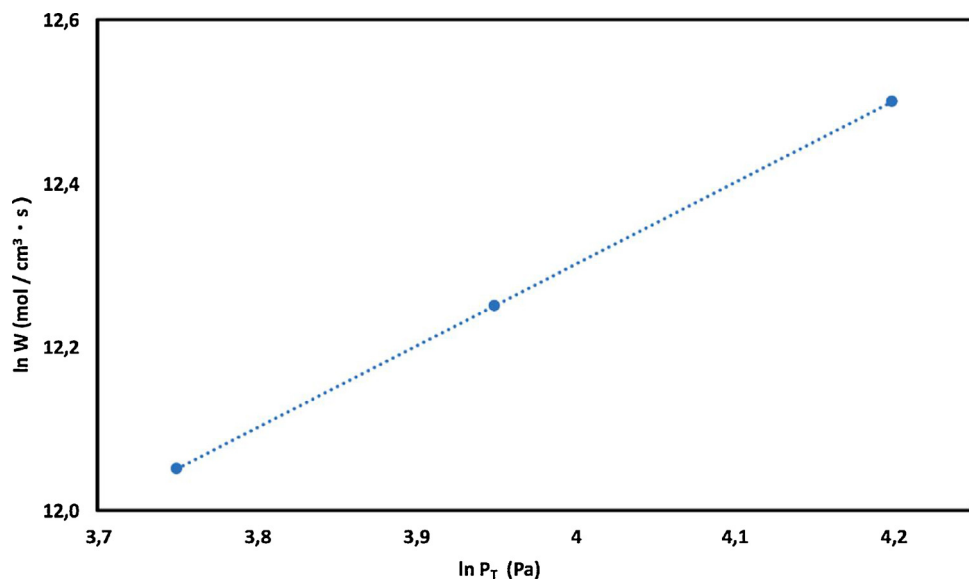


Fig. 10. Dependence of the rate of DCS formation on the vapor pressure ( $P_T$ ) of TCS in the initial gas mixture ( $T = 388$  K).

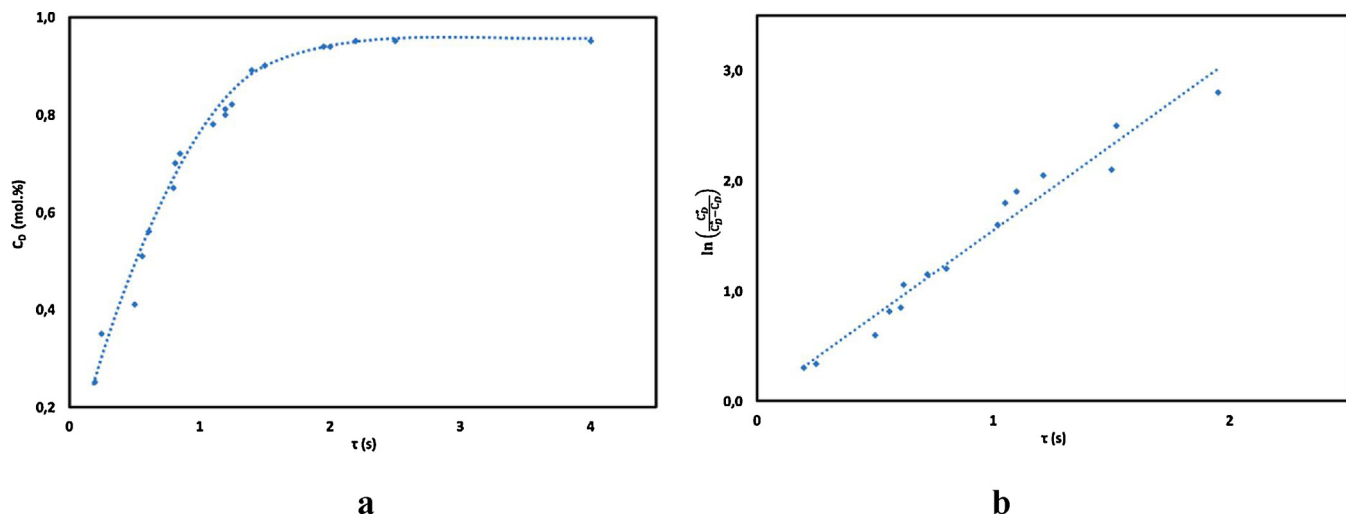


Fig. 11. The kinetics of DCS formation at the initial concentration TCS in the vapor gas mixture ( $T = 388$  K, Sample 6,  $C_{TCS} = 10$  mol. %).

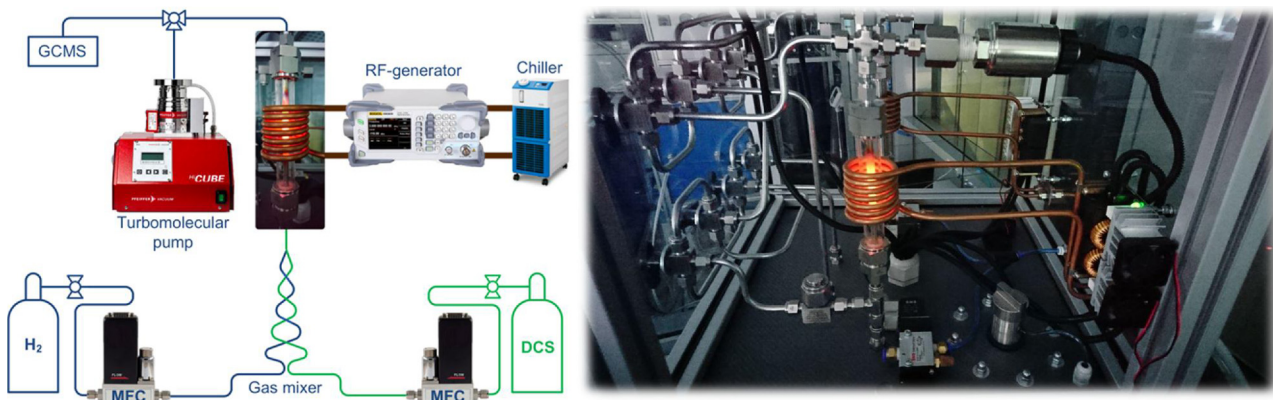


Fig. 12. Apparatus for DCS chemical vapor decomposition.

out by successive approximations before the convergence of the quasi-stationary equilibrium of the system.

From Fig. 3 it can be seen that the equilibrium yield of MS and MCS has a fairly low increase in the concentration at higher temperatures,

due to the low yield of the relevant products, but the increase in the concentration of DCS in the system occurs from 5 to 10%, which in turn is promising in terms of considering DCS as the main precursor for the processes of epitaxial silicon growth. In addition, the maximum

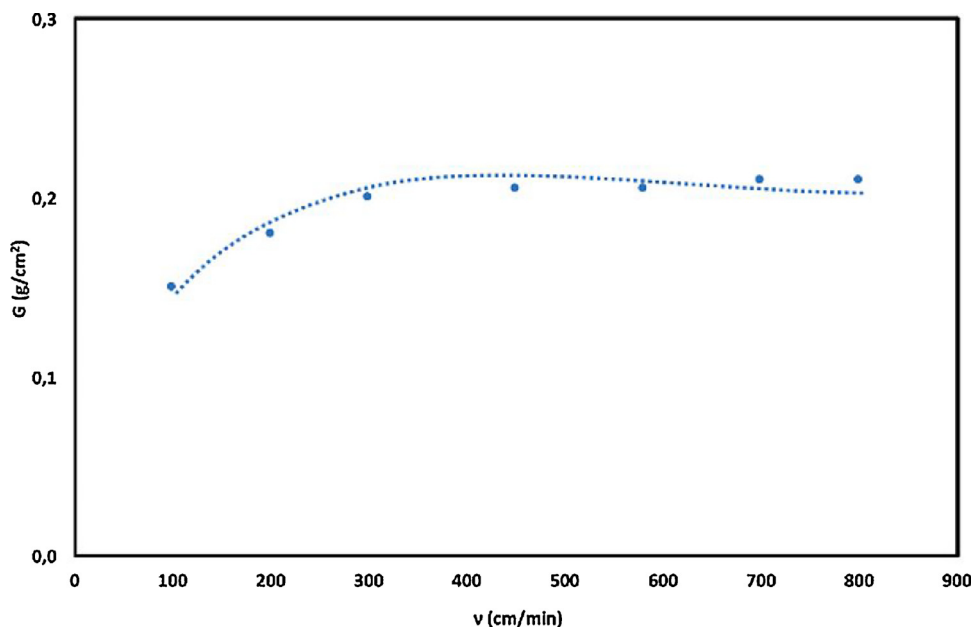


Fig. 13. The dependence of the deposition rate of silicon in the CVD of DCS from the flow rate of the gas mixture.

attainable temperature is thermodynamically optimal for the process.

### 3.2. SILC characterization

#### 3.2.1. The thermal stability of the SILC by Evolved Gas analysis (EGA)

The temperature stability of the DVB-CMS supports was determined using evolved gas analysis, the results are shown in Fig. 5. All samples with a different surface structure having the same nature of decomposition are subjected to deactivation by thermodegradation by hydrogen chloride ( $m/z$  36) formation in the first step and the destruction of a polymer matrix with toluene ( $m/z$  91) and m-vinyl ethyl benzene ( $m/z$  117) formation. All samples have a similar thermal stability 475 K. The decomposition start temperature was determined by method 3 of the sigma, at the time when the characteristic mass signal became 3 times higher than the background signal, the corresponding temperature was determined.

#### 3.2.2. SEM

The SEM images of the DVB-CMS microspheres were shown in Fig. 6. All of these polymer particles have nearly perfect spherical shape with non-segmented surfaces. The monodispersity was inherited when porous polymer microparticles were prepared. The nuclei were formed during the suspension polymerization most likely by the aggregation of oligomers at the initial stage. Then the particles were grown by the radical reaction with the formation of oligomers and comonomers subsequently. Monodisperse PS seed particles prepared by dispersion polymerization have an average diameter of 397  $\mu$ m, and the coefficient of variation (CV) is only about 3.7%

#### 3.2.3. Topography analysis by AFM

The topography map shows the microsphere surface has a loose structure with pronounced large-scale relief (Fig. 7). According to AFM scanning, an arithmetic average roughness height ( $R_a$ ) and a mean roughness depth ( $R_z$ ) were obtained. A base length (a length of a line used for roughness selection) was 3  $\mu$ m. Since the function of heights distribution (according to surface profile) is unimodal,  $R_a$  and  $R_z$  could be used as quantitative parameters of the surface irregularities. Wherein  $R_a$  correlates with an amplitude of the small-scale roughness, and  $R_z$  correlates with the large-scale one. From the results of the AFM analysis,  $R_a$  is about 20 nm, and  $R_z$  is about 100 nm.

The deflection map shows numerous dark areas, i.e., those with the

lowest heights. They were interpreted as pores. The pores had the shapes of conical capillaries. Their lateral sizes were determined by the surface micro profiles using the AFM software tools. The pore size was varied from 40 to 70 nm. With this pore size, the use of the chosen cantilever ruled out the effect of the contraction of profile valleys.

#### 3.2.4. Pore and surface structure characterization by the nitrogen physisorption

For pore structure analysis, the nitrogen adsorption-desorption isotherms were determined over the widest possible range of relative pressure. Obtained isotherms which attributed to Type IV are given by mesoporous samples. The adsorption behavior in mesoporous is determined by the adsorbent- adsorptive interactions and also by the interactions between the molecules in the condensed state and characterized by hysteresis in the 0.8–0.95 region  $P/P_0$ . In this case, the initial monolayer-multilayer adsorption on the mesoporous walls, which takes the same path as the corresponding part of a Type II isotherm, is followed by pore condensation. A typical feature of Type IV isotherms is a reduction to a mere inflection point in  $P/P_0 = 0.95$ . The hysteresis loops at moderate to high relative pressure, as shown in Fig. 8, indicate mesoporous structures of porous microspheres.

From the desorption isotherm (Fig. 8), the pore size distribution was obtained. The results indicate that a different ratio of monomers to porogen affects the pore diameter and, as a consequence, the specific surface area. Fig. 9b shows the distribution of pores (for a sample with 100% addition of porogen as an example), whose character is described by the Gaussian distribution with a maximum of 15 nm. The final results are shown in Table 1.

All structural characteristics depend on the ratio of monomers to porogen, with an increase in which the average pore diameter, specific surface area, and pore volume increase. The work studied only the effect of the porogen, but these characteristics are also affected by the ratio of DVB/CMS [43] and the ratio of the organic phase to the water phase.

### 3.3. Comparison of catalytic activities

#### 3.3.1. The kinetics of the reaction disproportionation of TCS

To compare the catalytic activity of different catalytic systems on the basis of macroporous supports modified by different tritic ammonium functional groups with the subsequent activation, the kinetics of

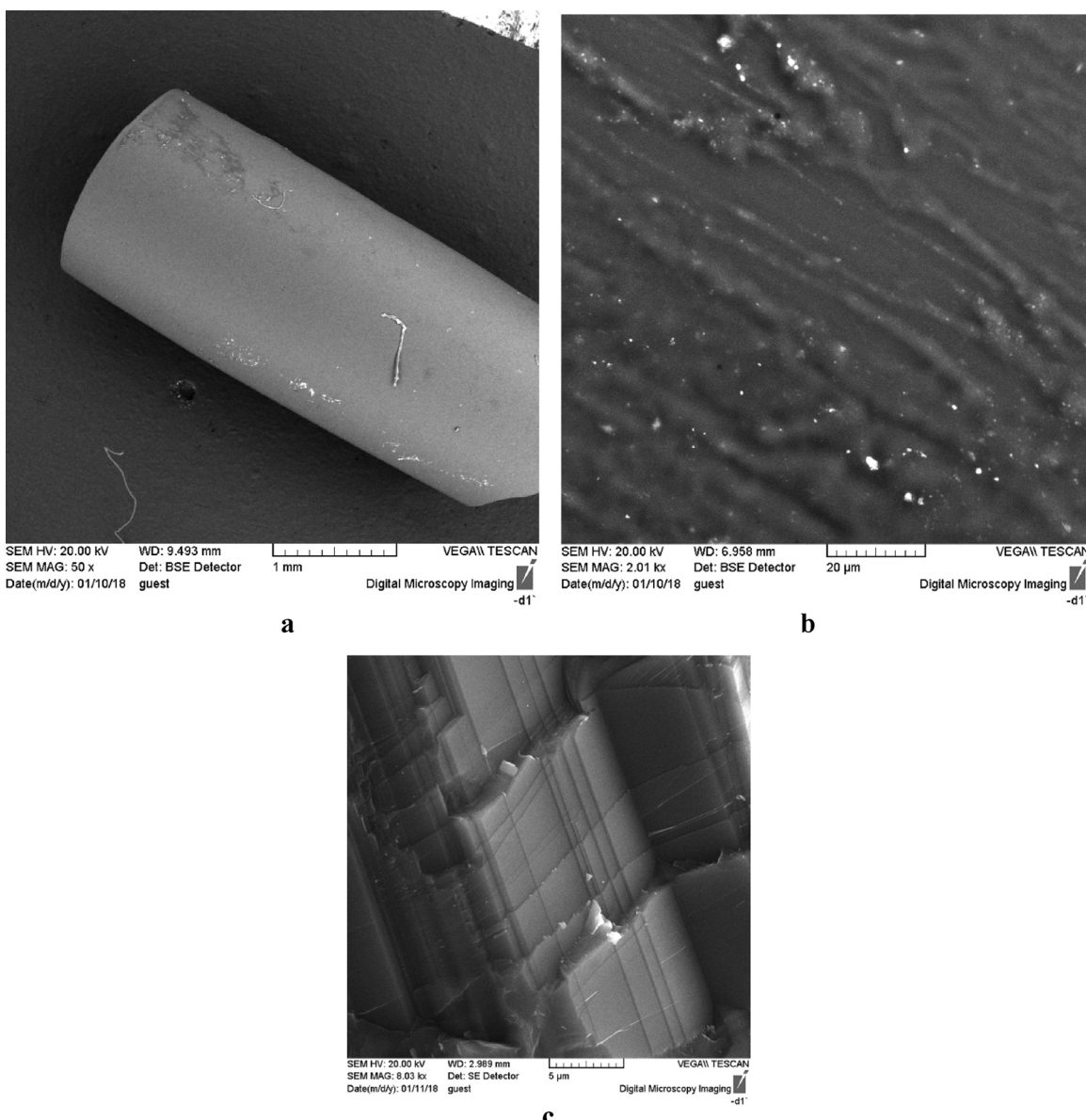


Fig. 14. SEM micrographs of the poly-Si after CVD (a – 50x side view, b – 2010x longitudinal corrugations, c – 8030x transverse cleavage).

the TCS disproportionation on the catalyst sample having the highest catalytic activity was studied, which was evaluated by the static method [46]. As the catalyst which was carried out for the kinetic studies was chosen Sample No. 6 from Table 2. A mixture of TCS with helium was fed to the reactor filled with a dehydrated catalyst sample. In order to determine the area in which the reaction is carried out, different variations of the catalyst were taken at a different flow rate of helium saturated with TCS vapor. The area in which the reaction takes place in the kinetic region was established, and diffusion restrictions do not affect the kinetics of the process. The qualitative and quantitative composition of the gas phase was determined by a chromato-mass spectrometry with absolute calibration.

Fig. 10 shows the experimental dependence of the rate of DCS formation on the TCS partial pressure in the initial gas mixture with a low degree of conversion (10%), which excludes the occurrence of temperature gradients. The value of the tangent of the inclination angle of the straight line allows us to conclude that the direct reaction (1) has the first order of the TCS ( $n = 0.942$ ).

Fig. 11 shows the dependence of the concentration of DCS on the contact time obtained for different catalyst amount (0.2; 0.6; 1.8;

2.5 cm<sup>3</sup>). All experimentally obtained points lie on the same curve, which indicates that with the same contact time, but different values of the flow rate linearly (differing by more than an order of magnitude), the rate of DCS formation does not change and the reaction takes place in the kinetic region, and external and internal diffusion does not affect the disproportionation process.

Based on Fig. 11a, the induction period of the reaction is an average of 2 s, after which the equilibrium degree of TCS conversion is achieved, however, if the pre-activate of the catalyst is not completed with hydrogen chloride or TCS, the induction period increases to 4 min for an overhang of 0.2 cm<sup>3</sup> due to the transition of non-activated functional fragments into a charged form. Assuming that the reverse process is also a first-order reaction, the kinetics of DCS formation should be described by the following equation,

$$\frac{dC_{DCS}}{d\tau} = K_1 (C_{\tau}^0 - 2C_{DCS}) - K_2 C_{DCS} \quad (5)$$

where  $C_{DCS}$  – concentration of DCS at the time,  $C_{\tau}^0$  – initial concentration of TCS at  $\tau = 0$ ,  $\tau$  – contact time.

By introducing the necessary assumption that the inverse reaction is

a reaction of the first order and integrating the equation on the catalyst layer, the following expression of the process velocity constant can be obtained:

$$\frac{C_{DCS}^*}{C_\tau^0} \ln \frac{C_{DCS}^*}{C_{DCS}^* - C_{DCS}} = K_1 \tau \quad (6)$$

where  $C_{DCS}^*$ ,  $C_{DCS}$  – equilibrium and current concentration of DCS.

This equation allows calculating from experimental data the constant of the speed of the process using different anions. Fig. 11b shows the graphical dependence of the equation (6), all the points lie in a straight line, which suggests that the equation describes the kinetics of the dispersion of TCS. The value of the velocity constant for the sample was found by the angle of inclination of the line and shown in Table 2.

### 3.3.2. Catalytic activity

The catalytic activity of SILLPs was determined at a constant initial concentration of TCS equal to 10 mol. %, and temperature 393 K. in accordance with 3.4.1. The value of the tangent of the inclination angle of the straight line is equal to the reaction rate constant, the values of which, referred to the unit of the catalyst volume, different samples of catalysts are shown in the Table 2.

To explain catalytic activity, first of all, it is necessary to compare the obtained results with the most important characteristics of the obtained systems: specific surface area, average pore diameter, exchange capacity and functional fragment. The table shows that catalytic activity, for all samples, depends on its specific surface area and, to a small extent, on the exchange capacity – the concentration of ionogenic groups. This is explained by the fact that the exchange capacity is an actual characteristic for liquid-phase processes where the swelling of the polymer matrix occurs, as a result of which the active centers of the entire volume become available. In the case of reactions in the gas phase, the interaction is limited only by the available functional groups, the availability of which increases with the increase in the area of the specific surface area. This dependence is clearly seen in samples with the same functional fragments, but different specific surfaces (table - 2). For example, for sample No. 4 and 6, changing the specific surface area from 3 to 79 m<sup>2</sup>/g causes the velocity constant to increase by two orders of magnitude. In this regard, the highest value of the velocity constant is recorded for the sample 6, characterized by the maximum value of these values.

On the other hand, the type of functional group plays an important role. Thus, if we compare samples 3, 6 and 9, we can see that the replacement of the functional group in the nitrogen atom leads to an increase in catalytic activity at close values of exchange capacity and specific surface area. This is especially evident in the transition from methyl to ethoxy radical, which increases the total charge of nitrogen. In addition, it is worth noting that sample No. 1 has low catalytic activity due to the complete closure of the nitrogen atom, as opposed to gel type samples 4 and 7. The results obtained indicate that the introduction of acceptor substituents increases catalytic activity in the disproportionation of TCS. In addition, the reason for the high catalytic activity of sample 6 may be due to the influence of ethoxy oxygen on the coordination of adsorption molecules. Based on the fact that the reaction mechanism can be represented as a nucleophilic substitution [46], in the case where the substitute nitrogen atom contains electro-negative atoms, such as oxygen atom, as a result of additional polarization increases the lability of chlorine and hydrogen atoms in the intermediate, which is formation on the active site.

## 3.4. Decomposition of DCS

### 3.4.1. Kinetics of decomposition of DCS

To assess the feasibility of using DCS as a raw material for the creation of semiconductor structures, the kinetics of thermal decomposition of DCS in a mixture with hydrogen was studied at a

temperature of 1200–1500 K. The experiments were carried out at the setup, the scheme of which is shown in Fig. 12.

The graph of the dependence of the specific rate of silicon deposition  $G$  on the rate of gas flow at a temperature of 1400 K is shown in Fig. 13. The figure shows that at a flow rate of more than 300 ml/min the process takes place in the kinetic region. According to the obtained kinetic results, the activation energy of the process is determined, which is in the temperature range of 1220–1320 K and the concentration of DCS in hydrogen 9–28.6 mol.%, is 112.9 kJ/mol. Activation energy value indicates the heterogeneous nature of the thermal decomposition.

### 3.4.2. SEM analysis

As a result of thermal deposition of DCS, a poly-Si sample in the form of a cylinder was obtained, according to scanning electron microscopy (Fig. 14), the resulting sample has a fairly homogeneous structure. When magnified 20,000 times, the longitudinal corrugations are visible on the part of the sample, which appears to be formed during cooling. The transverse chipped also looks fairly homogeneous and clearly traces the boundaries of the epitaxial layers.

Thus, it was shown that the use of DCS for the production of silicon reduces the energy costs in the process of silicon deposition by reducing the pyrolysis temperature by 150–200 K at a higher degree of silicon extraction compared to the process of its production from a mixture of TCS with hydrogen. The deposition rate of silicon can be increased in 2 times compared to TCS. These factors, along with the possibility of obtaining DCS in a high-purity state, make it one of the promising sources of high-purity silicon.

## 4. Conclusion

In the presented work developed a method of disproportionation of trichlorosilane on the supported ionic liquid-like phases based on CMS/DVB with different NR<sub>3</sub> cation as catalysts. To determine the optimal conditions for conducting a complex catalytic process, the primary task is to determine the thermodynamical equilibrium state of the reaction system. It was shown that the concentration of DCS in the equilibrium mixture increases with the temperature and is practically independent of the pressure and phase composition of the system. the increase in the concentration of DCS in the system occurs from 5 to 10%, which in turn is promising in terms of considering DCS as the main precursor for the processes of epitaxial silicon growth. In addition, the maximum attainable temperature is thermodynamically optimal for the process.

DVB/CMS copolymer beads were obtained by suspension copolymerization and direct functionalized by 3-types of cations (Me<sub>2</sub>NH<sup>+</sup>, Me<sub>3</sub>N<sup>+</sup> and Me<sub>2</sub>EtON<sup>+</sup>). The use of SEM and AFM showed that polymer particles have nearly perfect spherical shape with non-segmented surfaces and an average diameter of 397 μm and the coefficient of variation (CV) is only about 3.7%. According to AFM scanning, an arithmetic average roughness height and a mean roughness depth were obtained. For pore structure analysis, the nitrogen adsorption-desorption isotherms were determined over the widest possible range of relative pressure. From the desorption isotherm, the pore size distribution was obtained. The results indicate that a different ratio of monomers to porogen affects the pore diameter and, as a consequence, the specific surface area.

The kinetics of the TCS disproportionation on the catalyst sample having the highest catalytic activity was studied. The results obtained indicate that the introduction of acceptor substituents increases catalytic activity in the disproportionation of TCS. To explain catalytic activity, first of all, it is necessary to compare the obtained results with the most important characteristics of the obtained systems: specific surface area, average pore diameter, exchange capacity and functional fragment. In the case of reactions in the gas phase, the interaction is limited only by the available functional groups, the availability of which increases with the increase in the area of the specific surface

area. This dependence is clearly seen in samples with the same functional fragments, but with different specific surfaces. Furthermore, the type of functional group plays an important role. The results obtained indicate that the introduction of acceptor substituents increases catalytic activity in the disproportionation of TCS. In addition, the reason for the high catalytic activity of sample with  $\text{Me}_2\text{EtON}^+$  cation may be due to the influence of ethoxyl oxygen on the coordination of adsorption molecules, in the case where the substitute nitrogen atom contains electronegative atoms, such as oxygen atom, as a result of additional polarization increases the lability of chlorine and hydrogen atoms in the intermediate, which is formation on the active site.

To assess the feasibility of using DCS as a raw material for the creation of semiconductor structures, the kinetics of thermal decomposition of DCS in a mixture with hydrogen was studied at a temperature of 1200–1500 K. According to the obtained kinetic results, the activation energy of the process is determined, which is in the temperature range of 1220–1320 K and the concentration of DCS in hydrogen 9–28.6 mol.%, is 112.9 kJ/mol. Activation energy value indicates the kinetical mode of the thermal decomposition. Thus, it was shown that the use of DCS for the production of silicon reduces the energy costs in the process of silicon deposition by reducing the pyrolysis temperature by 150–200 K at a higher degree of silicon extraction compared to the process of its production from a mixture of TCS with hydrogen.

## Acknowledgments

This work was financially supported by the Russian Science Foundation, grant No. 17-73-20275 “Highly selective catalyst systems for the processes of low-temperature disproportionation, hydrogenation and reduction of chlorosilanes: Synthesis, properties, mechanism and application”).

## References

- [1] S.H. Ahn, D.M. Chun, W.S. Chu, *Int. J. Precis. Eng. Manuf. Technol.* 14 (6) (2013) 873–874.
- [2] <https://www.pv-tech.org/editors-blog/100gw-of-pv-modules-to-ship-during-2018-but-is-quality-matching-quantity-pa>.
- [3] A.V. Shah, J. Meier, E. Vallat-Sauvain, et al., *Sol. Energy Mater. Sol. Cells* 78 (1) (2003) 469–491.
- [4] Y. Nishi, R. Doering, *Handbook of Semiconductor Manufacturing Technology*, CRC Press, 2007 1720 p.
- [5] S. Chu, A. Majumdar, *Nature* 488 (7411) (2012) 294–303.
- [6] B.R. Bathey, M.C. Cretella, J. Mater. Sci. 17 (11) (2005) 3877–3896.
- [7] W.C. O’Mara, R.B. Herring, L.P. Hunt, *Handbook of Semiconductor Silicon Technology*, Noyes Publications, New Jersey, 1990 795 p.
- [8] M.A. Green, *Sol. Energy* 76 (1–3) (2004) 3–8.
- [9] M.J.-P. Duchemin, M.M. Bonnet, M.F. Koelsch, *J. Electrochem. Soc.* 125 (1978) 637–644.
- [10] A. Luque, S. Hegedus, *Handbook of Photovoltaic Science and Engineering*, John Wiley & Sons, 2011 1162 p.
- [11] A.V. Vorotyntsev, S.V. Zelentsov, V.M. Vorotyntsev, *Russ. Chem. Bull.* 60 (8) (2011) 1531–1536.
- [12] S.K. Iya, R.N. Flagella, F.S. Dipaolo, *J. Electrochem. Soc.* 129 (1982) 1531–1535.
- [13] A.V. Vorotyntsev, G.M. Mochalov, V.M. Vorotyntsev, *Inorg. Mater. Appl. Res.* 49 (1) (2013) 1–5.
- [14] K. Yasuda, T.H.J. Okabe, *Jpn. Inst. Met.* 74 (2010) 1–9.
- [15] A.V. Vorotyntsev, A.N. Petukhov, I.V. Vorotyntsev, T.S. Sazanova, M.M. Trubyanov, I.Y. Kopersak, E.N. Razov, V.M. Vorotyntsev, *Appl. Catal. B: Environ.* 198 (2016) 334–346.
- [16] S. Liu, W. Xiao, *Chem. Eng. Sci.* 127 (2015) 84–94.
- [17] Experimental Process System Development Unit for Producing Semiconductor Silicon Using Silane-to-Silicon Process / Union Carbide Corp. Final Report, DOE/JPL Contract 954334, National Technical Information Center, Springfield, VA, 1981.
- [18] V.M. Vorotyntsev, Method for the production of silanes. RU 2152902, 20 Jule 2000.
- [19] M. Mehler, *Electron. News* 30 (1485) (1984) 54.
- [20] J.K. Iya, *J. Cryst. Growth* 75 (1986) 88–90.
- [21] V.M. Vorotyntsev, G.M. Mochalov, O.V. Nipruk, *Russ. J. Appl. Chem.* 74 (4) (2001) 621–625.
- [22] J. Harada, Process for production of silane. U.S. Patent 4,704,264, 3 November 1987.
- [23] X. Huang, W.-J. Ding, J.-M. Yan, W.-D. Xia, *Ind. Eng. Chem. Res.* 52 (18) (2013) 6211–6220.
- [24] J.R. Alcántara-Avila, H.A. Sillas-Delgado, J.G. Segovia-Hernández, *Comput. Chem. Eng.* 78 (2015) 85–93.
- [25] W.-J. Ding, J.-M. Yan, W.-D. Xiao, *Ind. Eng. Chem. Res.* 53 (27) (2014) 10943–10953.
- [26] I. Zaidi, Y.-H. Jang, D.G. Ko, I.-T.J. Im, *Crystal Growth* 483 (2018) 1–8.
- [27] C. Álvarez-Maciás, J.D. Escobar-Carrasquilla, A. Dutt, E. Mon-Pérez, L. González, G. Santana, *Nano* 12 (11) (2017) 1750134.
- [28] C. Ramírez-Márquez, E. Sánchez-Ramírez, J.J. Quiroz-Ramírez, F.I. Gómez-Castro, N. Ramírez-Corona, J.A. Cervantes-Jauregui, J.G. Segovia-Hernández, *Chem. Eng. Process. Process. Intensif.* 108 (2016) 125–138.
- [29] H. Song, M.V.S. Chandrashekhar, T.S. Sudarshan, *ECS J. Solid State Sci. Technol.* 4 (3) (2015) P71–P76.
- [30] A.A. Zagorodni, *Ion Exchange Materials: Properties and Applications*, Elsevier, 2007 477 p.
- [31] C.J. Bakay, Process for making silane. U.S. Patent 3,968,199, 6 Jule 1976.
- [32] L.M. Coleman, Process for the production of ultrahigh purity silane with recycling from separation columns. U.S. Patent 4,340,574, 20 Jule 1985.
- [33] S. Morimoto, Process for the disproportionation of chlorosilanes. U.S. Patent 4,613,489, 23 September 1986.
- [34] J-K. Lepage, G. Soula, Process for the disproportionation of silanes. U.S. Patent 4,548,917, 22 October 1985.
- [35] C.J. Litteral, Process for preparing disproportionation products of chlorosilanes. DE Patent 2162537, 24 February 1977.
- [36] T. Bauer, R. Stepic, P. Wolf, F. Kollhoff, W. Karawacka, C.R. Wick, M. Haumann, P. Wasserscheid, D.M. Smith, A.-S. Smith, J. Libuda, *Catal. Sci. Technol.* 8 (1) (2018) 344–357.
- [37] A.I. Akhmetshina, A.N. Petukhov, A.V. Vorotyntsev, A.V. Nyuchev, I.V. Vorotyntsev, *ACS Sustain. Chem. Eng.* 5 (4) (2017) 3429–3437.
- [38] M.I. Burguete, H. Erythropel, E. García-Verdugo, S.V. Luis, V. Sans, Green, *Chemistry* 10 (4) (2008) 401–407.
- [39] P. Lozano, E. García-Verdugo, R. Piamtongkam, N. Karbass, M.I. Burguete, S.V. Luis, J.L. Iborra, *Adv. Synth. Catal.* 349 (2007) 1077–1084.
- [40] M.H. Valkenberg, C. deCastro, W.F. Hölderich, *Green Chem.* 4 (2002) 88–93.
- [41] M.I. Burguete, F. Galindo, E. García-Verdugo, N. Karbass, S.V. Luis, *Chem. Commun. (Camb.)* 29 (2007) 3086–3088.
- [42] A. Kirschning, W. Solodenko, K. Mennecke, *Chem.–Eur. J.* 12 (2006) 5972–5990.
- [43] Lu Li, Jiang Cheng, Xiufang Wen, Pihui Pi, Zhiuru Yang, *Chinese J. Chem. Eng.* 14 (4) (2006) 471–477.
- [44] ASTM-D1895, Apparent Density, Bulk Factor and Pourability of Plastic Materials. Annual Book of ASTM Standards, Part 35, Plastics General Test Methods, Nomenclature, ASTM, 1979.
- [45] W.T. Thomson, *Philos. Mag.* 42 (1871) 448.
- [46] A.V. Vorotyntsev, A.N. Petukhov, D.A. Makarov, E.N. Razov, I.V. Vorotyntsev, A.V. Nyuchev, N.I. Kirillova, V.M. Vorotyntsev, *Appl. Catal. B: Environ.* 224 (2018) 621–633.